UNIVERSITY OF LEEDS

This is a repository copy of *An analytical geometrical model for secondary dendrite arm detachment*.

White Rose Research Online URL for this paper:
http://eprints.whiterose.ac.uk/84398/

Version: Accepted Version

Article:
Mullis, AM (2006) An analytical geometrical model for secondary dendrite arm detachment. Scripta Materialia, 54 (5). 795 - 799. ISSN 1359-6462

https://doi.org/10.1016/j.scriptamat.2005.11.022

© 2006, Elsevier. Licensed under the Creative Commons Attribution-NonCommercial-NoDerivatives 4.0 International http://creativecommons.org/licenses/by-nc-nd/4.0

Reuse
Unless indicated otherwise, fulltext items are protected by copyright with all rights reserved. The copyright exception in section 29 of the Copyright, Designs and Patents Act 1988 allows the making of a single copy solely for the purpose of non-commercial research or private study within the limits of fair dealing. The publisher or other rights-holder may allow further reproduction and re-use of this version - refer to the White Rose Research Online record for this item. Where records identify the publisher as the copyright holder, users can verify any specific terms of use on the publisher's website.

Takedown
If you consider content in White Rose Research Online to be in breach of UK law, please notify us by emailing eprints@whiterose.ac.uk including the URL of the record and the reason for the withdrawal request.

White Rose university consortium
Universities of Leeds, Sheffield & York

eprints@whiterose.ac.uk
https://eprints.whiterose.ac.uk/

An Analytical Geometrical Model for Secondary Dendrite Arm Detachment

Andrew M. Mullis

Institute for Materials Research,
University of Leeds,
Leeds LS2 9JT,
UK.

Keywords: Solidification microstructure; casting; modelling; dendrite detachment.

Abstract

A simple geometrical model of a ripened secondary dendrite arm is used to investigate the curvature at the neck of the arm where it joins the primary trunk. It is found that the negative $K^{(1)}$ component of the curvature does not fully balance the peak in the positive $K^{(2)}$ component.

Introduction

Within the mushy zones of a solidifying metallic melt a number of complex interactions between the growing dendrites and their parent melt can occur as a result of natural or forced flow. One such interaction is the copious detachment of secondary dendrite arms. These dendritic fragments may subsequently be swept by the flow away from the mushy zone towards the centre of the casting, where they may act as powerful heterogeneous nuclei, leading to grain multiplication and ultimately a grain refined microstructure. In deed, a number of aluminium producers have experimented with the viability of using mechanical agitation during the DC casting process as an alternative to the addition of chemical grain refiners to the melt [1].

However, despite the potential commercial importance of dendrite fragmentation and detachment as a result of flow in the parent melt, the phenomenon is far from well understood. Fig. 1 shows a dendrite grown [2] in the transparent analogue system NH_4Cl-H_2O. Many of its secondary arms display the familiar geometry characteristic of alloy systems, being highly constricted at the base where they join the primary

dendrite trunk. This geometry is usually attributed to the initial growth phase of the secondary arm as it grows through the solute rich boundary layer adjacent to the primary trunk. These features appear delicate in the extreme, yet it is well established that in quiescent conditions they may persist for long periods of time as relatively stable features [3, 4]. However, if perturbed by motion of the parent melt detachment may occur.

Several mechanisms have been proposed to account for the detachment of secondary dendrite arms in a flow. These include [5, 6] local remelting due to warm fluid being swept over the dendrites, mechanical shearing, plastic deformation followed by remelting and constitutional remelting. The latter may occur because the high solute concentration in the boundary adjacent to the primary trunk will lower the local melting temperature. If the solute concentration is altered by the flow the local melting temperature will drop and remelting may occur [7].

According to the Gibbs-Thomson relationship, the equilibrium solute concentration in the liquid is increased by the curvature of the dendrite by an amount

$$c_l - c_l^r = -\frac{\sigma T}{Hm} K \tag{1}$$

where c_l is the equilibrium concentration at a flat interface, c_l^r is the local equilibrium concentration, σ the surface energy between the solid and liquid phases, T the absolute melting temperature, H the heat of fusion per unit volume, m is the slope of the liquidus line and K is the curvature. For a body which is a figure of revolution, K will have two components, $K^{(1)}$ and $K^{(2)}$ ($K = K^{(1)} + K^{(2)}$) the orientation of which are shown in Fig. 2. It is generally accepted that the high $K^{(2)}$ component of the curvature that results due to the narrow neck of the secondary arm is balanced by the negative $K^{(1)}$ component of the curvature [5]. If this were not the case the large positive $K^{(2)}$ component of the curvature at the neck of the secondary arm would lead to rapid remelting due to the increased local solubility in this region.

Any viable mechanism for secondary arm detachment must be able to account for a number of observations that have been made relating to this phenomenon, in particular those of Glicksman & co workers [6] on the succinonitrile-acetone system. By observing the detachment of dendrites in a controlled flow cell and making simultaneous measurements of the local flow velocity in the mushy zone they found that increasing the flow velocity does not necessarily increase the fragmentation rate and, moreover, that detachment often occurs in swarms, that is there is a critical level of disturbance at which large numbers of dendrite arms will detach essentially simultaneously.

In this paper we examine the morphology of ripened secondary dendrite arms in the NH_4Cl-H_2O analogue casting system and apply a simple analytical model to calculate the $K^{(1)}$ and $K^{(2)}$ component of the curvature to establish the extent that these are in fact in balance and thus comment on the viability of various detachment mechanisms.

Method

In order to model the $K^{(1)}$ and $K^{(2)}$ components of the curvature we have used a geometrical model of a ripened secondary arm that we have previously employed to model fluid flow within the mushy zone [8, 9]. The primary requirements of the geometrical model are that the dendrite arm, which we take to have unit height, should have a smooth, continuously differentiable surface with a radius minimum r_1, at a height z_1, and a radius maximum r_2, at height z_2 (see Fig. 2).

The following parametric function can be shown to satisfy these criteria

$$\overline{\mathbf{Z}}(t,\theta) = \begin{pmatrix} r(t)\cos(\theta) \\ r(t)\sin(\theta) \\ z(t) \end{pmatrix} \qquad 0 \le \theta \le 2\pi \qquad (2)$$

where

$$r = a_0(a_1 t + a_2 t^2 + a_3 t^3 + a_4 t^4) \qquad t \ge 0 \qquad (3)$$

$$z = \exp(-t^2) \qquad t \geq 0 \tag{4}$$

Here a_i (i = 0, 4) are parameters which are determined by the values of (r_1, z_1) and (r_2, z_2) according to

$$a_0 = \left(\alpha^2\beta^2\left(3\alpha\beta(\alpha-\beta)+\beta^3-\alpha^3\right)\right)^{-1} \tag{5}$$

$$a_1 = 2\alpha\beta(\beta^4 r_1 - \alpha^4 r_2) + 4\alpha^2\beta^2(\alpha^2 r_2 - \beta^2 r_1) \tag{6}$$

$$a_2 = \alpha^5 r_2 - \beta^5 r_1 + \alpha\beta\left(\alpha^3 r_2 - \beta^3 r_1 + 8\alpha\beta(\beta r_1 - \alpha r_2)\right) \tag{7}$$

$$a_3 = 2(\beta^4 r_1 - \alpha^4 r_2) + 4\alpha\beta\left(\alpha^2 r_2 - \beta^2 r_1 + \alpha\beta(r_2 - r_1)\right) \tag{8}$$

$$a_4 = \alpha^3 r_2 - \beta^3 r_1 + 3\alpha\beta(\beta r_1 - \alpha r_2) \tag{9}$$

$$\alpha = \sqrt{-\ln(z_1)} \tag{10}$$

$$\beta = \sqrt{-\ln(z_2)} \tag{11}$$

In applying this parametric form to model the geometry of secondary dendrite arms the main underlying assumptions are that each individual secondary arm can be considered as a figure of revolution and that the parametric form is itself a good representation of the profile of the arm. The first of these appears reasonable provided we restrict consideration to secondary arms that are themselves not undergoing tertiary arm growth. Theoretically this approach can be justified by the low crystalline anisotropy of most metals. Although growth process tend to amplify crystalline anisotropy exponentially this is not true of ripening and remelting processes. The fact that the morphology of secondary dendrite arms (in the absence of tertiary growth) is governed principally by ripening rather than growth processes [10, 11] mean that they are likely to be figures of revolution to a good approximation. The second assumption can be justified empirically by comparing the model geometry

to that of real secondary arms. As shown in the insert in Fig. 1, provided we again restrict our consideration to secondary arms without tertiary branching the assumption appears valid. That is, provided we fit the model to the co-ordinates of the radius minimum and maximum, (r_1, z_1) and (r_2, z_2) respectively, a good approximation to the actual geometry of a ripened secondary dendrite arm is obtained.

In order to determine realistic values of the parameters (r_1, z_1) and (r_2, z_2) we have made careful measurements of these parameters on 34 of the best developed secondary arms apparent in Fig. 1. The arms selected for this process are indicated in the figure. We acknowledge that the solid fraction for the NH_4Cl-H_2O system shown in Fig. 1 is very low, leading to secondary arms that are likely to be relatively longer and more slender than those in most metallic castings, nonetheless the *mechanism* stabilising the secondary arms in this system is likely to be the same as that operating in metallic systems at higher solid fraction.

The rationale for selecting the arms chosen is relatively straightforward. Firstly, we have avoided arms within 40 visible sidebranches of the tip, to ensure that the geometry we are studying is indicative of the ripening and not the growth process and secondly have selected only the larger arms for inclusion within the data set. The reasons for this latter condition are twofold. Firstly the numerous small sidebranches evident along the length of the dendrite are likely to be being actively removed, a process which occurs by axial dissolution causing the dendrite to shrink from its tip back towards its root rather than to detach from the trunk [12]. Secondly, and perhaps more pragmatically, it is easier to make the measurements accurately for the larger sidebranches.

For each of the 34 sidebranches selected the parametric geometrical model has been fitted to the measured values of (r_1, z_1) and (r_2, z_2) and Mathematica [13] has been used to calculate the differentials, r_t, z_t, r_{tt} and z_{tt} from which it is then a fairly straightforward matter to calculate z_r and z_{rr} and hence $K^{(1)}$ and $K^{(2)}$ from their standard forms,

$$K^{(1)}(z,r) = \frac{z_{rr}}{(1+z_r^2)^{3/2}} \tag{12}$$

$$K^{(2)}(z,r) = \frac{z_r}{r\sqrt{1+z_r^2}} \tag{13}$$

Results

Figures 3 a&b shows the values of r_i and z_i as a function of L, the length of the corresponding dendrite. In line with the definitions of r and z above, the measured radii and heights have been non-dimensionalised by dividing by L. With reference to Figure 3a we note that, both r_1 and r_2 show a systematic tendency to decrease with increasing L. In deed, to a reasonable first approximation trend lines fitted through the two data sets would be parallel. In contrast, z_1 and z_2 appear to be independent of L, although the data for z_2 shows considerable scatter. The implication of this is that, unlike the case for *growth* of a dendrite, secondary dendrite arms are not self-similar to within a characteristic length scale. They become instead relatively more slender as they become longer, although the locations of the maximum and minimum radii do not appear to change with length. This no doubt reflects the fact that the morphology of secondary dendrite arm is governed by ripening as opposed to growth processes [10, 11]. For the 34 sidebranches measured the mean location of the maximum and minimum radii are $\bar{z}_1 = 0.07 \pm 0.02$ and $\bar{z}_2 = 0.59 \pm 0.07$.

Figure 4 shows a typical profile for the curvatures $K^{(1)}$ and $K^{(2)}$, in this case calculated for a dendrite with dimensions $(\bar{r}_1, \bar{z}_1)$ and $(\bar{r}_2, \bar{z}_2)$, where for reference the mean values of r_1 and r_2 are $\bar{r}_1 = 0.03$ and $\bar{r}_2 = 0.08$. In keeping with the co-ordinate system described above the curvature is given in dimensionless units. For a secondary arm of average length, $\bar{L} \approx 190\,\mu\text{m}$, the maximum in $K^{(2)}$ of 34 would equate to a positive curvature of 1.7×10^5 m^{-1}. It is clear from Fig. 4 that, as would be expected, there is a sharp positive peak in the $K^{(2)}$ component of the curvature in the vicinity of the radius minimum at z_1, which is balanced by a negative peak in the $K^{(1)}$ component. However, it is significant that the positive peak in $K^{(2)}$ is not completely balanced by the negative peak in $K^{(1)}$. In fact in the case illustrated the relative magnitudes are $K^{(1)}_{\min} = -27$ and $K^{(2)}_{\max} = 34$.

We have performed the type of calculation illustrated in Fig. 4 separately for each of the 34 measured sidebranches and the results for $K_{\min}^{(1)}$ and $K_{\max}^{(2)}$, together with their summation, are displayed in Fig. 5. Here, because each of the sidebranches has a different length, we have reverted to using dimensional curvature in order that a meaningful comparison can be made. Despite considerable scatter in the data, which is probably indicative of the fact that some of the sidebracnches are actively dissolving while other are growing, the general picture is that the total curvature in the vicinity of the radius minimum is generally positive, i.e. as above the negative $K^{(1)}$ component does not fully balance $K^{(2)}$. The mean total curvature in the vicinity of r_1 is $\overline{K} = 4.1\times10^{4}$ m^{-1}.

As described by Equation (1), this residual curvature at the neck of the sidebranch gives rise to a local solubility in the liquid of c_l^r , which will be higher than the equilibrium solubility c_l. Consequently, if rapid remelting of the sidebranch at its root is not to occur the actual local concentration of solute in the liquid must be close to c_l^r. This local concentration in the liquid will in turn be established by equilibrium with the local vicinity of the secondary arm and the primary trunk to which it attaches.

To estimate the local concentration of solute in the liquid we have assumed that this is governed solely by exchange with the local vicinity of the secondary arm. Consequently, the local mean concentration of solute in the liquid, $\overline{c}_l$, will be determined by the mean curvature of the arm over some characteristic diffusion length, d_l. That is

$$\overline{c}_l = c_l + \frac{\sigma T}{Hm}\overline{K} \qquad (14)$$

where $\overline{K}$ is the mean curvature in the vicinity of the radius minimum, which is given by

$$\overline{K} = \frac{\int_{z_1-d_l}^{z_1+d_l} r(K^{(1)} + K^{(2)})\,\partial z/\partial t \;\mathrm{d}t}{\int_{z_1-d_l}^{z_1+d_l} r\,\partial z/\partial t \;\mathrm{d}t} \tag{15}$$

The problem now reduces to estimating the characteristic diffusion length, d_l. However, as the narrowing of the root of the secondary arm in the vicinity of the primary trunk is itself a manifestation of it growing through a solute boundary layer we may take the height of the radius minimum as being indicative of the characteristic length scale for solute diffusion. With $\bar{z}_1$ being 0.07 we have taken the limits on the integral as being (in dimensionless units) 0 to 0.15 approximately, wherein, for our average dendrite defined by a minimum ($\bar{r}_1$, $\bar{z}_1$) and a maximum ($\bar{r}_2$, $\bar{z}_2$) the integral evaluates to $\overline{K} = 8.6$. Re-dimensionalising against the average length, $\overline{L} = 190\,\mu\mathrm{m}$, the gives a mean curvature of $\overline{K} = 4.6\times10^4$ m^{-1}, in remarkably close agreement with the average difference between of $K^{(2)}_{\max}$ and $K^{(1)}_{\min}$.

Discussion

From the above calculation, we would conclude that although the enhanced solubility occasioned by the high $K^{(2)}$ component of the curvature is not exactly cancelled by the negative $K^{(1)}$ component, the small positive residual leads to a solubility at the neck which is very close to the local concentration of solute in the liquid as established by equilibrium between the solid and liquid averaged over some typical diffusion length scale, d_l. This would very naturally explain both why these apparently delicate features can persist for relatively long time under quiescent conditions but are subject to detachment in swarms if there is flow in the interdendritic liquid. Specifically, if the fluid local to the vicinity of the neck of the sidebranch, with solute concentration close to c_l^r is replaced by fluid with containing the equilibrium solute concentration, c_l, remelting will occur essentially simultaneously at all sidebranches. Moreover, as shown in Figure 6 this is likely to be a runaway process. In Figure 6 we have plotted the effect on $K^{(1)}$ and $K^{(2)}$ of the effect of a small change in r_1, on the assumption that L, z_1 and z_2 remain unchanged. At the radius minimum at z_1, $K^{(2)}$ is only dependant upon r_2, but $K^{(1)}$ depends on the geometry of the whole dendrite and may

consequently be effected by possible changes in r_2. We have considered three possible scenarios regarding r_2 during this process (i) that it remains constant, (ii) that it changes at the same rate as r1, (iii) the relative rates of change of r_1 and r_2 are proportional to the local curvature at these points, i.e. $\delta r2/\delta r1 = K(z_2)/K(z_1)$, although in fact for the particular case considered the differences between the three scenarios are so small as to not be distinguishable when plotted on Figure 6. For this example calculation we have used the values of $\bar{z}_1$, $\bar{r}_2$ and $\bar{z}_2$, with a starting value for r_1 of $\bar{r}_1$, and a starting value for r_2 of $\bar{r}_2$. What is evident from the figure is that $K^{(1)}$ is relatively insensitive to changes in r_1 (and r_2) while $K^{(2)}$ increases rapidly as r_1 decreases. That is even a small amount of remelting is likely to drive the system further from equilibrium, thus accelerating the rate of remelting. Detachment of secondary arms in a swarm would invariably follow.

References

1 C Vives, *Int. J. Heat Mass Transf.* **33** (1990) 2585.

2 J Pilling & A Hellawell, *Metall. Mater. Trans. A* **27** (1996) 229.

3 A Hellawell, in 'Modelling of casting, welding and advanced solidification process, Vol. VII' (eds. Cross & Campbell) 1995, TMS, Warrendale, pp. 565-576.

4 GC Hansen, A Hellawell, SZ Lu & RS Steube, *Metall. Mater. Trans.* **27** (1996) 569.

5 A Hellawell, in ' Proc. 4th Int. Conf. on Semi-Solid Processing of Alloys & Composites' (eds. Kirkwood & Kapranos) 1996, University of Sheffield, Sheffield UK, pp. 60-65.

6 PGN Rao, ME Glicksman, RN Smith & GM Knott, in ' Proc. 4th Decennial Int. Conf. on Solidification Processing ' (eds. Beech & Jones), 1997, University of Sheffield, Sheffield UK, pp. 417-421.

7 KA Jackson, JD Hunt, DR Uhlmann & TP Seward, *Trans. Metall. Soc. AIME* **236** (1966) 149.

8 K Dragnevski, AM Mullis, DJ Walker & RF Cochrane, *Acta Mater.* **50** (2002) 3743.

9 AM Mullis, DJ Walker, SE Battersby & RF Cochrane, *Adv. Eng. Mater.* **2** (2000) 597.

10 K.P. Young & D. H. Kirkwood, *Met. Trans.* **6A** (1975), 197.

11 AM Mullis, *Acta Mater.* **46** (1998) 4609.

12 D.H. Kirkwood, *Mater. Sci. Eng.* **73** (1985), L1.

13 Mathematica is a product of Woolfram Research Ltd., Champaign IL.

Figures

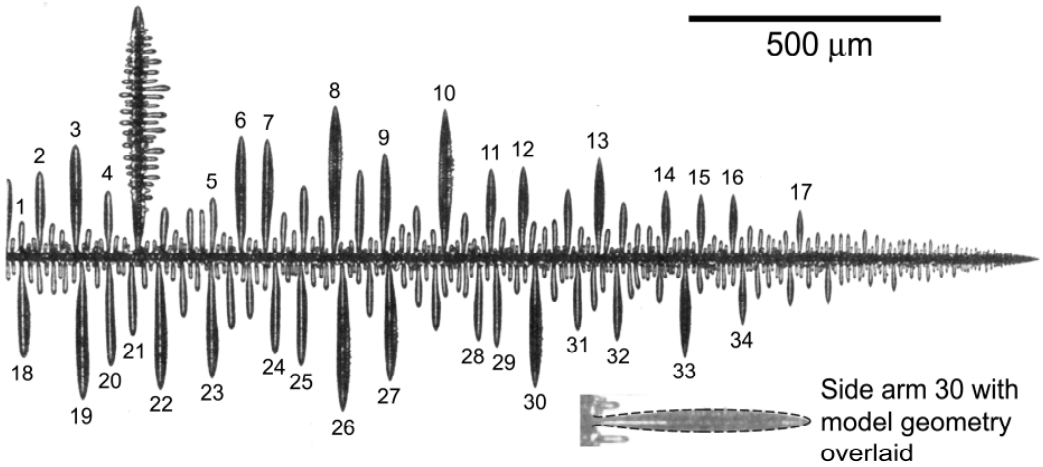

Fig. 1. Image of a dendrite grown in the analogue casting system NH_4Cl-H_2O [from Ref. 2]. Note that many of its secondary arms display the familiar geometry characteristic of alloy systems, being highly constricted at the base. The numbers indicate those secondary arm for which measurements of the radius and location of the maximum and minimum diameters were made. The insert shows an example of the model geometry adopted in the work overlaid upon one of the dendrite sidebranches from the image.

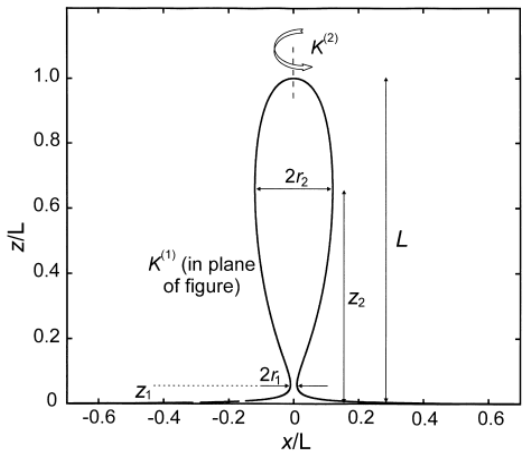

Fig. 2. Geometrical model of a ripened secondary arm, also illustrating the orientations of the $K^{(1)}$ and $K^{(2)}$ components of the curvature.

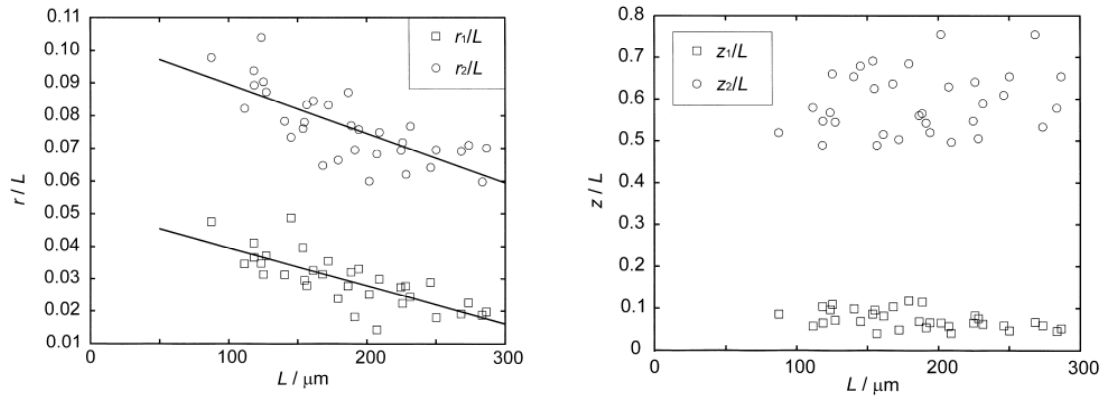

Fig. 3. The radii (a) and position (b) of the maximum and minimum diameters for 34 of the best developed secondary dendrite arms in Fig. 1, shown as a function of the length of the arm, *L*.

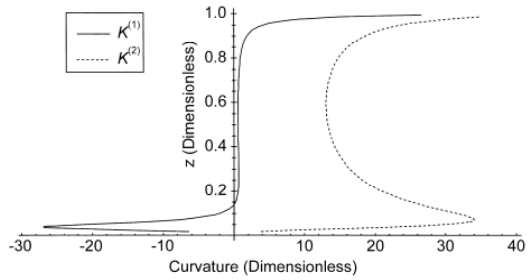

Fig. 4. Illustrative calculation of the $K^{(1)}$ and $K^{(2)}$ components of the curvature along the length of an average secondary dendrite arm. Note that minimum in the negative $K^{(1)}$ component does not fully cancel the peak in the $K^{(2)}$ component.

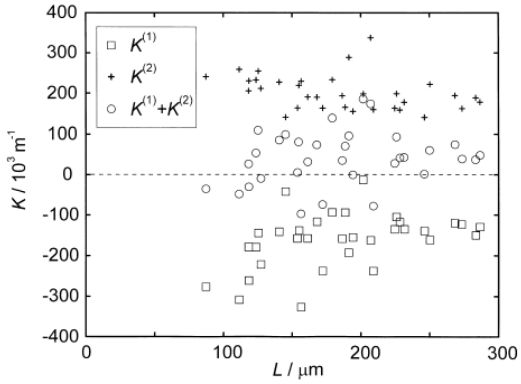

Fig. 5. The values of the minimum in the $K^{(1)}$ and maximum in the $K^{(2)}$ components of the curvature in the vicinity of the radius minimum near where the secondary arm joins the primary trunk of the dendrite.

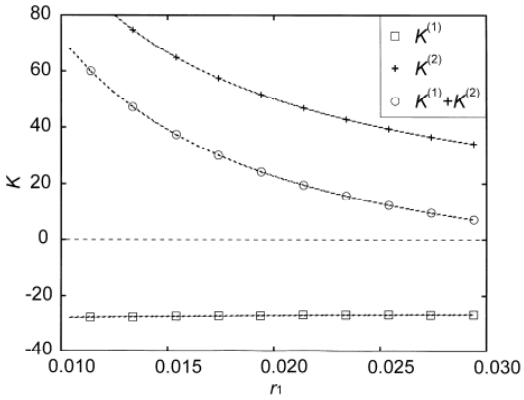

Fig. 6. Illustrative calculation of how the minimum in the $K^{(1)}$ and maximum in the $K^{(2)}$ components of the curvature in the vicinity of the radius minimum near where the secondary arm joins the primary trunk of the dendrite vary as a function of r_1.